NUMERICAL SIMULATION OF LOCAL SCOUR PROCESS DUE TO SUBMERGED JET DOWNSTREAM OF A GROUNDSILL

Tatsuhiko Uchida[(1)], Shoji Fukuoka[(2)]

[(1)] Department of Social and Environmental Engineering, Graduate School of Engineering, Hiroshima University, 1-4-1 Kagamiyama, Higashi-hiroshima, 739-8527, Japan,
phone: +81 82 424 7847, fax: +81-82-424-7847, e-mail: utida@hiroshima-u.ac.jp
[(2)] Research and Development Initiative, Chuo University, 1-3-1 Kasuga, Bunkyo-ku, Tokyo, 112-8551, Japan,
phone: +81-3-3817-1625, fax: +81-3-3817-1625, e-mail: sfuku@tamacc. ac.jp

ABSTRACT

Local scours downstream of groundsills undermine the foundation of the structure. There are two different processes of local scour downstream of groundsills due to the flow over the structure. The duration of the developing process due to submerged jet is so short that our interest is only in the deformation of scour shape and the maximum scour depth. In this study, scour shape deformation process is computed by the equilibrium sediment transport model because of its simplicity, not emphasizing the rate of absolute sediment transport. The vertical two-dimensional model for the flow in the local scour has been developed, which employs sigma coordinate system to take into account of the variation of water surface, bed height. We confirmed that the model can compute both the scour processes under the submerged jet flow and wave jump flow. And it is found that the maximum local scour depth by the experiment is reproduced by the computation.

Keywords: scour process, maximum scour depth, vertical two-dimensional model, submerged jet flow, wave jump flow, sediment transport

1 INTRODUCTION

Local scours just downstream of structures may undermine their foundations, revetment works and levees. Since complete protection against local scour is almost impossible, a reliable design method by the prediction of the maximum depth and the shape of local scour is highly required to minimize the damage of the structure. To this end, it is necessary to clarify the flow field and the local scouring just downstream of the structure based on experiments and numerical simulations.

Local scouring is a complex phenomenon depending on the flow characteristics. It develops owing to the turbulence of a hydraulic jump [Farhoudi and Smith (1985)], the turbulence downstream of bed protective works [Hoffmans (1993) and Kanda *et al*. (1996)] and at the presence of plunging jet. Local scour downstream of a groundsill, which is the main topic in this study, is caused by a submerged jet, a type of plunging jet. Most of the studies dealing with the prediction of the local scour at the presence of plunging jets have been carried out experimentally [Stein *et al.* (1993), Bormann and Julien (1991), Hoffmans (1998), Mazurek and Rajatnam (2005)]. Their prediction methods are relatively simple and practical. However, the applicability of their methods to scour depth downstream of a groundsill is not clear, because the flow pattern downstream of the structure varies considerably according to the bed deformation. Hence, a numerical model which can simulate both flow and sediment transport is to be refined. Kawashima and Fukuoka (1995) developed a two-dimensional numerical model for shallow water flow to compute the bed variation around a groundsill. Their model, however, did not reproduce the local scour well, because the model did not take into account of the vertical fluid motions and pressure distribution.

There are two different processes of local scouring downstream of a groundsill(see Fig.1). These phenomena are the same as reported by Suzuki *et. al* (1982). One is a developing

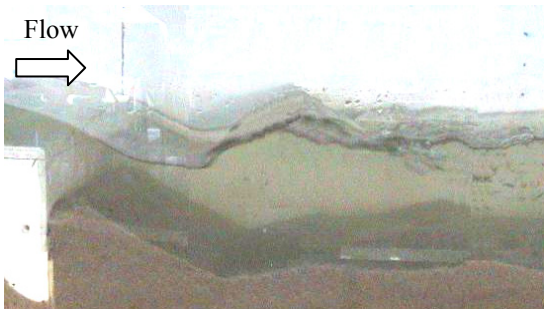

(a) Decaying process under wave-jump flow

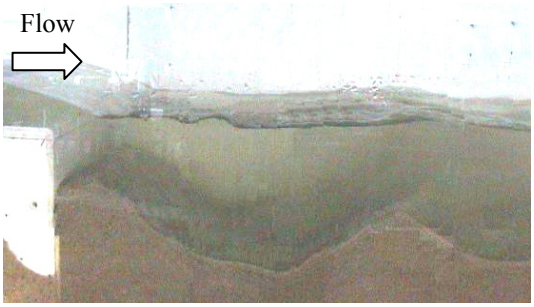

(b) Developing process under submersed-jet flow

Fig.1 The process of local scouring just downstream of a groundsill

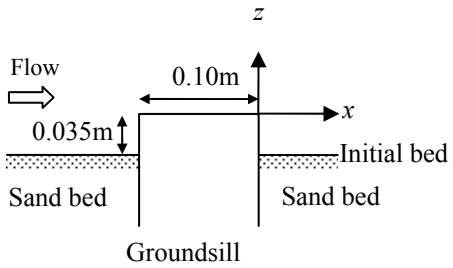

Fig.2 The view of the groundsill installed in the channel

Table 1 Experimental conditions

Channel length	8.0 m
Channel width	0.30 m
Initial bed slope	1/166.7
Experimental discharge	0.0072 m3/s
Water depth at downstream end	0.054 m
Diameter of sand bed	0.8 mm

process where the local scour enlarges by the action of the submerged jet flow. This is important to design the structures, because the maximum scour depth is generated in this process. Stein *et al.* (1993) pointed out that the sediment transport under plunging jet is greatly different from that in equilibrium flow. Non-equilibrium sediment transport with a lot of suspended sediment can be seen in Fig.1(b). Traditional sediment transport models such as Meyer and Peter-Muller formula do not correctly estimate the sediment transport from the local scour. Jia *et. al* (2001) considers the non-equilibrium sediment transport and fluctuating lift force acting on the sand in their sediment transport model. However, the duration of the developing process is so short that the main interest lies not in the speed of bed deformation but in the shape and the maximum depth of the scour.

In the following, a numerical model for the flow in the local scour is developed to compute longitudinal bed shear distribution reasonably with a sediment transport model to discuss the deformation of local scour shape. The reliability of the present model is discussed through the comparison with the experimental data.

2 EXPERIMENT

To understand the mechanism of a local scour downstream of a groundsill and to verify the performance of the numerical model, an experiment is conducted. Table 1 shows the experimental conditions. A groundsill is installed in the experimental channel as shown in Fig.2. The top of the groundsill is set 0.035 m above the initial bed for the bed scour. The bed shear is not beyond the critical tractive force upstream of the groundsill and no sediment is supplied from upstream of the scour in the experiment.

A local scour develops after sufficient time and two different scour processes appear alternately. One is a developing process under a submersed jet flow and the other is a decaying process with a wave jump flow. These processes were recorded by digital video camera. Fig.1 shows two different processes in the experiment. Velocity components are measured using an electro-magnetic velocimetry.

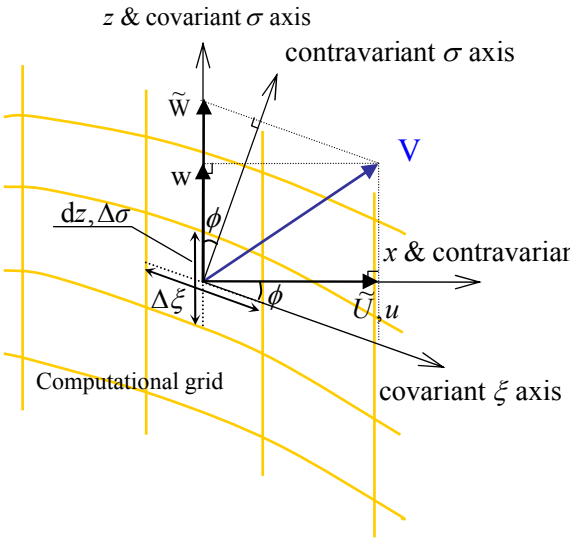

$$d\sigma = \Delta\sigma \cdot \cos\phi \qquad d\xi = \Delta\xi \cdot \cos\phi$$

$$\begin{pmatrix} \tilde{U} \\ \tilde{W} \end{pmatrix} = \begin{pmatrix} 1 & 0 \\ -\tan\phi & 1 \end{pmatrix} \begin{pmatrix} u \\ w \end{pmatrix}$$

$\Delta\xi, \Delta\sigma (= dz)$: grid spaces of covariant ξ, σ axis

$d\xi, d\sigma$: grid spaces of contravariant ξ, σ axis

u, w : fluid velocity of x, z component

$\tilde{U}$: fluid velocity of contravariant ξ component

$\tilde{W}$: fluid velocity of covariant σ component

Fig.3 The definition of the sigma coordinate system

3 NUMERICAL MODEL

The governing equations in the present numerical model are expressed in the sigma coordinate system to take into account of the variation of water surface and bed shape. A vertical two-dimensional model is developed. Fig.3 explains the sigma coordinate system where the covariant ξ-axis can be taken in the optional direction and the covariant σ-axis in the vertical direction (z-axis). Many models that use the body fitted coordinate system, have defined the vectors in the computational space. In the present model, however, vectors are defined in the physical space to easily specify the proper boundary conditions. Fig.3 also shows the vectors in the sigma coordinate system in the physical space. The momentum equations and the continuity equation are written as in Eqs.(1) ,(2) and (3).

$$\frac{\partial u}{\partial t} + \tilde{U}\frac{\partial u}{\partial \tilde{\xi}} + \left(\tilde{W} - w_g\right)\frac{\partial u}{\partial z} = -\frac{1}{\rho}\left(\frac{\partial p}{\partial \tilde{\xi}} - \tan\phi\frac{\partial p}{\partial z}\right) + \frac{1}{d\xi dz}\left\{\frac{\partial}{\partial \xi}\left(dz\tilde{\tau}_{\xi\xi}\right) + \frac{\partial}{\partial \sigma}\left(d\xi\tilde{\tau}_{\xi\sigma}\right)\right\} \tag{1}$$

$$\frac{\partial w}{\partial t} + \tilde{U}\frac{\partial w}{\partial \tilde{\xi}} + \left(\tilde{W} - w_g\right)\frac{\partial w}{\partial z} = -g - \frac{1}{\rho}\frac{\partial p}{\partial z} + \frac{1}{d\xi dz}\left\{\frac{\partial}{\partial \xi}\left(dz\tilde{\tau}_{z\xi}\right) + \frac{\partial}{\partial \sigma}\left(d\xi\tilde{\tau}_{z\sigma}\right)\right\} \tag{2}$$

$$\frac{\partial}{\partial \xi}\left(dz\tilde{U}\right) + \frac{\partial}{\partial \sigma}\left(d\xi\tilde{W}\right) = 0 \tag{3}$$

Here,

$\frac{\partial}{\partial \tilde{\xi}} = \frac{\partial}{d\xi \cdot \partial \xi}$, $\frac{\partial}{\partial z} = \frac{\partial}{dz \cdot \partial \sigma}$, p: pressure, $\tilde{\tau}_{ij}$: shear stress tensor given by Eq. (4), w_g : moving grid velocity in the vertical direction.

$$\begin{cases} \tilde{\tau}_{\xi\xi} = 2\nu_t\left(\dfrac{\partial u}{\partial \tilde{\xi}} - \tan\phi\dfrac{\partial u}{\partial z}\right) \\ \tilde{\tau}_{\xi\sigma} = -\tan\phi\tilde{\tau}_{\xi\xi} + \tilde{\tau}_{z\xi} \\ \tilde{\tau}_{z\xi} = \nu_t\left\{\dfrac{\partial u}{\partial z} + \dfrac{\partial w}{\partial \tilde{\xi}} - \tan\phi\dfrac{\partial w}{\partial z}\right\} \\ \tilde{\tau}_{z\sigma} = \nu_t\left\{\dfrac{\partial \tilde{W}}{\partial z} - \tan\phi\dfrac{\partial w}{\partial \tilde{\xi}} + \dfrac{1}{\cos^2\phi}\left(\dfrac{\partial w}{\partial z} + u\dfrac{\partial \phi}{\partial z}\right)\right\} \end{cases} \tag{4}$$

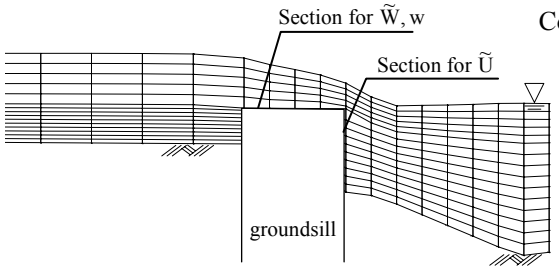

Fig.4 An example of the computational grid in the sigma coordinate system

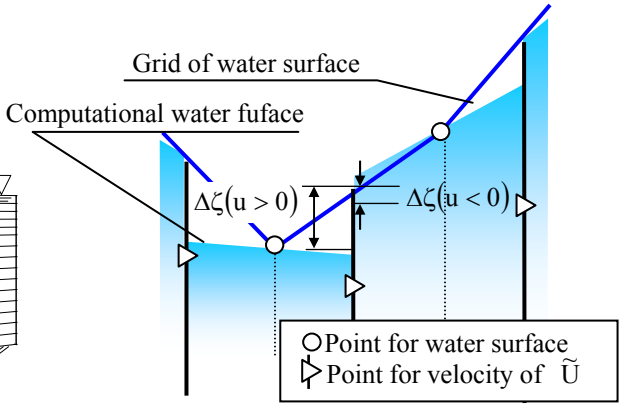

Fig.5 Cross-sectional area of passing through fluid

ν_t is given by Eq. (5), which is based on Smagorinsky (1963).

$$\nu_t = (C_s \Delta)^2 \cdot |\bar{S}| \tag{5}$$

Here,

$$\Delta = \sqrt{d\xi \cdot dz}, \quad |\bar{S}| = \left(2\tilde{S}_{\xi\xi} \frac{\partial u}{\partial \tilde{\xi}} + 2\tilde{S}_{\xi\sigma} \frac{\partial u}{\partial z} + 2\tilde{S}_{z\xi} \frac{\partial w}{\partial \tilde{\xi}} + 2\tilde{S}_{z\sigma} \frac{\partial w}{\partial z} \right)^{\frac{1}{2}}, \quad \tilde{\tau}_{ij} = 2\nu_t \tilde{S}_{ij}, \quad C_s = 0.2$$

Governing equations are solved by the finite difference method, using the staggered grid system. Fig.4 shows an example of the computational grid. An upwind scheme of the third order accuracy is used for the convection terms in the ξ direction. The other terms are discretized using the central differencing scheme of the second order accuracy. The pressure field is calculated with a HSMAC scheme (Hirt and Cook, 1972). The level of water surface and the vertical velocity on the water surface are calculated together with the pressure, using the continuity equation integrated over the water depth and the kinematics boundary condition at the water surface. Shear stresses acting on the bed and the groundsill are determined by applying the logarithmic law for rough beds at the node nearest to the relevant boundaries. The computational grid is reconstructed at each time step. The Heun method of the second order accuracy is adopted for the time integration.

Water surface in the control volume is depicted by the straight line of the average water surface gradient. However, the grid line of the water surface, which is constructed by connecting the averaged water surfaces in the control volume, is different from the computational water surface, as shown in Fig.5. In the present model, cross-sectional area for the fluid to pass through is introduced. To compute the fluid transport terms in the ξ direction at the top control volume, vertical sectional length $dz'=dz+\Delta\zeta$ is used instead of dz. There are two computational water surfaces at the cross-section accounting the ξ direction velocity. $\Delta\zeta$ is calculated by the upstream water surface, because the fluid is transported from the upstream. The above method is also adopted in the calculation near the bed. As in the case of water surface, two computational bed levels are defined at the cross-section. The higher bed level of the two is used, because the fluid cannot pass through the bed.

As the boundary conditions, the discharge is given at the upstream end and the water depth at the downstream end of the channel.

4 CALCULATION OF THE FLOW FIELDS IN LOCAL SCOUR

In the downstream of a groundsill, wave-jump and submersed-jet are alternated corresponding to the bed variation as shown in Fig.1. Numerical models have to reproduce these phenomena. The present model is at first checked whether it can generate two different

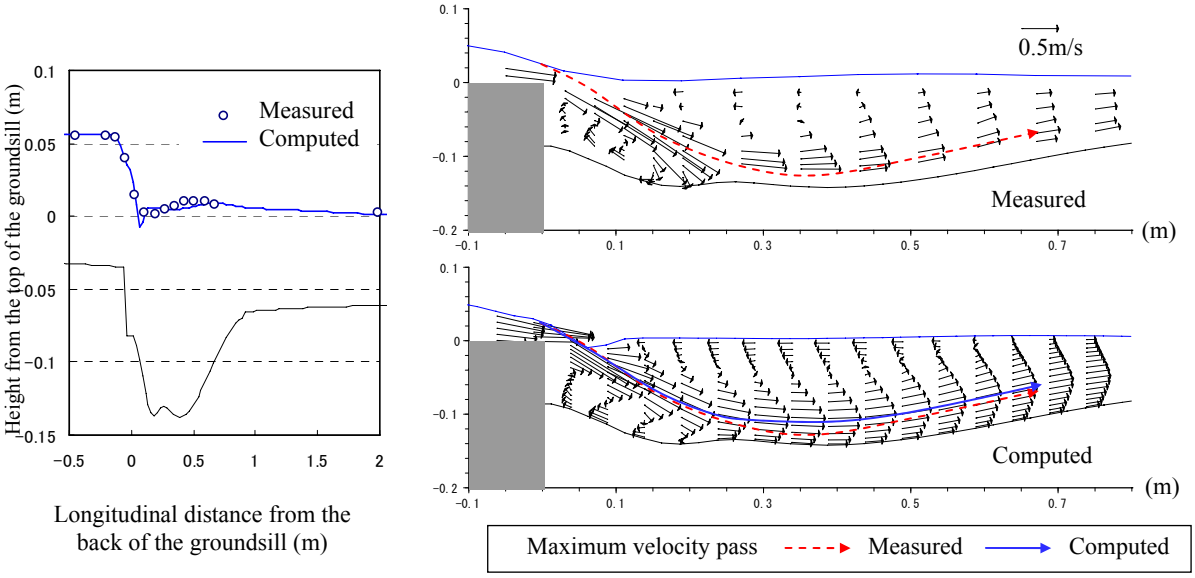

(a) Comparison of water surface (b) Comparison of velocity distribution

Fig.6 Comparison of the flow field for submersed-jet between measured and computed result

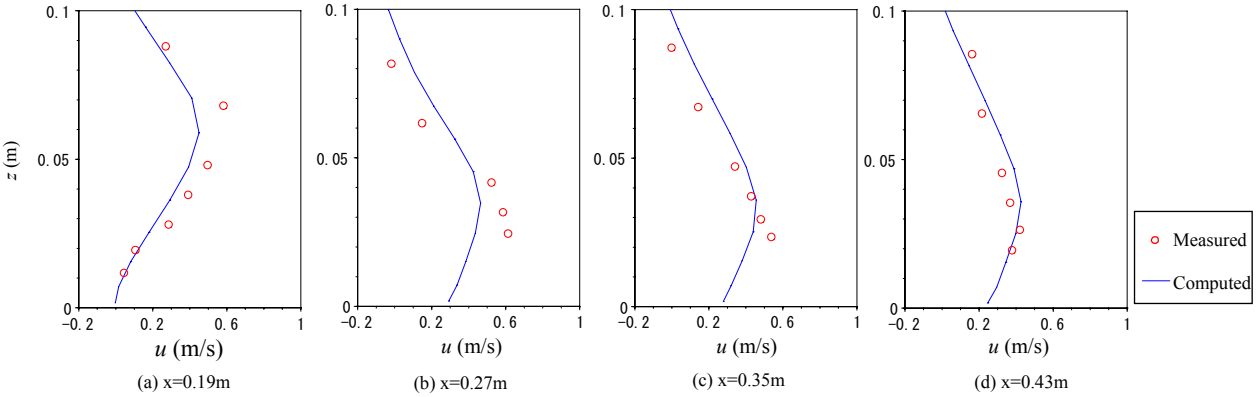

(a) x=0.19m (b) x=0.27m (c) x=0.35m (d) x=0.43m

Fig.7 Comparison of streamwise velocity distribution between measured and computed results

flows. In order to calculate two different flows generated under the same hydraulic conditions, initial condition and computation method are changed. For the calculation of a wave jump flow, the flow develops in the condition of high water-depth at downstream end, then the water-depth at downstream end is decreased to that in the experiment. On the other hand, for the calculation of submerged-jet flow, the submersed-jet flow is established in the condition of low water-depth at downstream end, then the water-depth at downstream end is increased to that in the experiment.

Fig.6 shows the comparison of (a) longitudinal water surface profiles and (b) velocity vectors in the local scour between measured and computed results at the presence of submersed jet flow. The flow over the groundsill runs into the water surface. At the downstream of a groundsill, high velocity occurs near the bed and recirculating flow near the water surface. These important flow characteristics in the local scour are well explained by the present model. Fig.7 shows the comparison of the vertical distribution of x-direction velocity between measured and computed results. Although the computed results show slightly different values, the present model gives good agreement with measured velocity distributions.

Fig.8 shows the comparison of (a) longitudinal water surface profiles and (b) velocity vectors in the local scour for the case of wave-jump flow. The flow past the groundsill runs

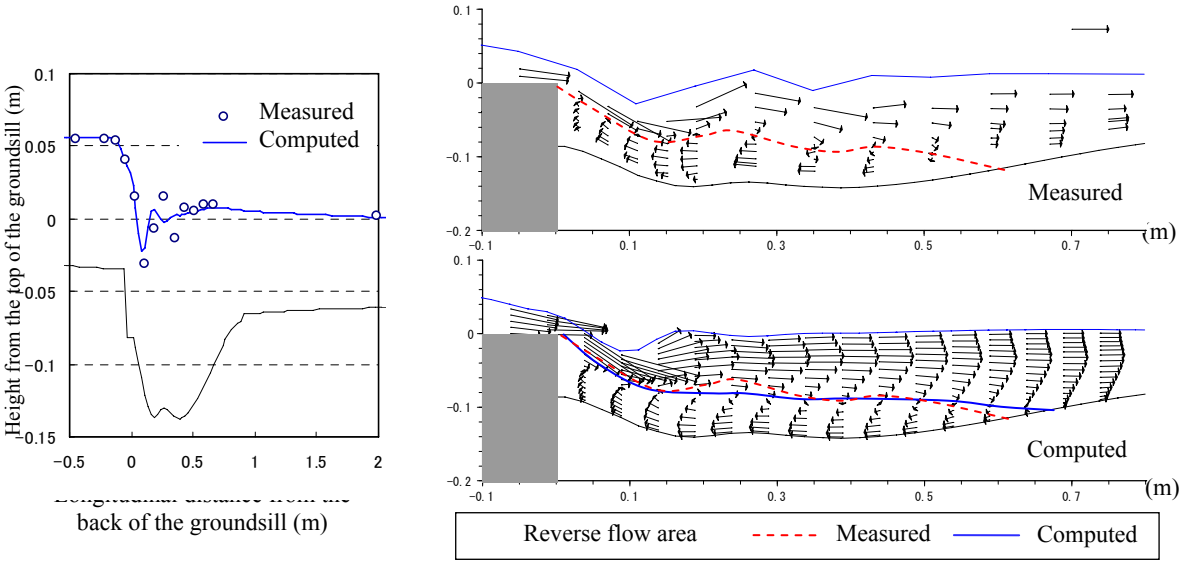

(a) Comparison of water surface (b) Comparison of velocity distribution

Fig.8 Comparison of the flow field for wave jump flow between measured and computed result

along the water surface, forming standing waves. For the wave-jump flow, a large area of the reverse flow is produced near the bed. The accuracy of the calculated result near water surface is not good. Since a wave-jump flow can coexist with a submersed-jet flow, water surface is unstable. In the computation under such condition, the velocity under water surface is decreased as shown in Fig.8, and then the flow becomes stable and a small wave-jump is produced. Although a finite differences scheme of the third order accuracy is used for convective terms, the numerical viscosities stemming from the sigma coordinate system and calculation method adopted under the water surface are not negligible to calculate the flow near the abrupt change of the water surface. However, the velocity near the bed, which plays an important role to induce a local scour, is almost reproduced by the present model.

The above results demonstrate that the coexistence of a wave jump and a submersed jet flow is satisfied in this model. Because the model explains the two different characteristics of the velocity distribution near the bed well, the model can be applied to calculate the local scour just downstream of a groundsill.

5 CALCULATION OF SCOUR PROCESS DUTE TO SUBMERGED JET

The performance of the present model is tested against the experimental results. Sediment transport rate from the local scour bed under submerged jet flow is different from that computed by the equilibrium sediment transport model owing to the pressure fluctuations and the suspended sediment. In fact, the absolute sediment transport rate and the deformation speed of the scour obtained by the following computation is underestimated by one tenth of those of the experiments. To improve this situation, the law of the wall on roughness bed and sediment transport model are modified. However, the duration of the submerged jet flow is so short that the emphasis is not placed on the speed of bed deformation rather on the scour shape deformation and the maximum scour depth.

Scour shape deformation is computed by an equilibrium sediment transport model of Ashida and Michiue formula (1972), taking into account of the gravity effect by the critical tractive force on inclined bed and additional tractive force due to gravity [Fukuoka and Yamasaka (1983)]. The moving grid speed on the bed, which is a part of the convective velocity in the sigma direction (see Eq.(3)), is calculated by the continuity equation for the sediment. If the angle of the bed surface is calculated beyond its repose angle, the bed surface

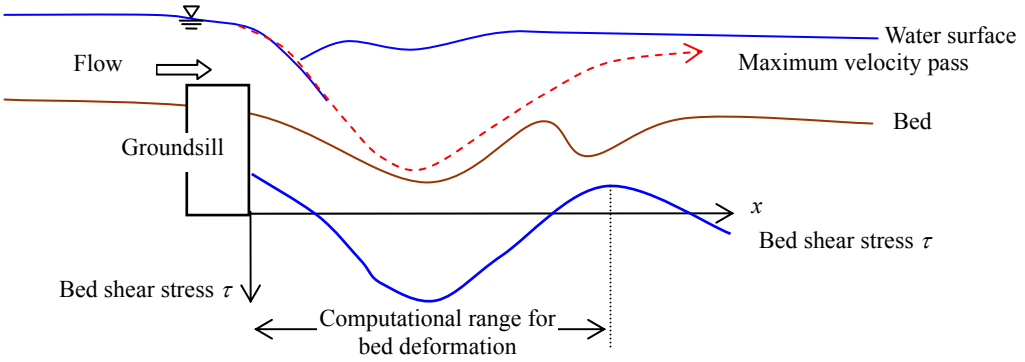

Fig.9 Computational range for bed deformation

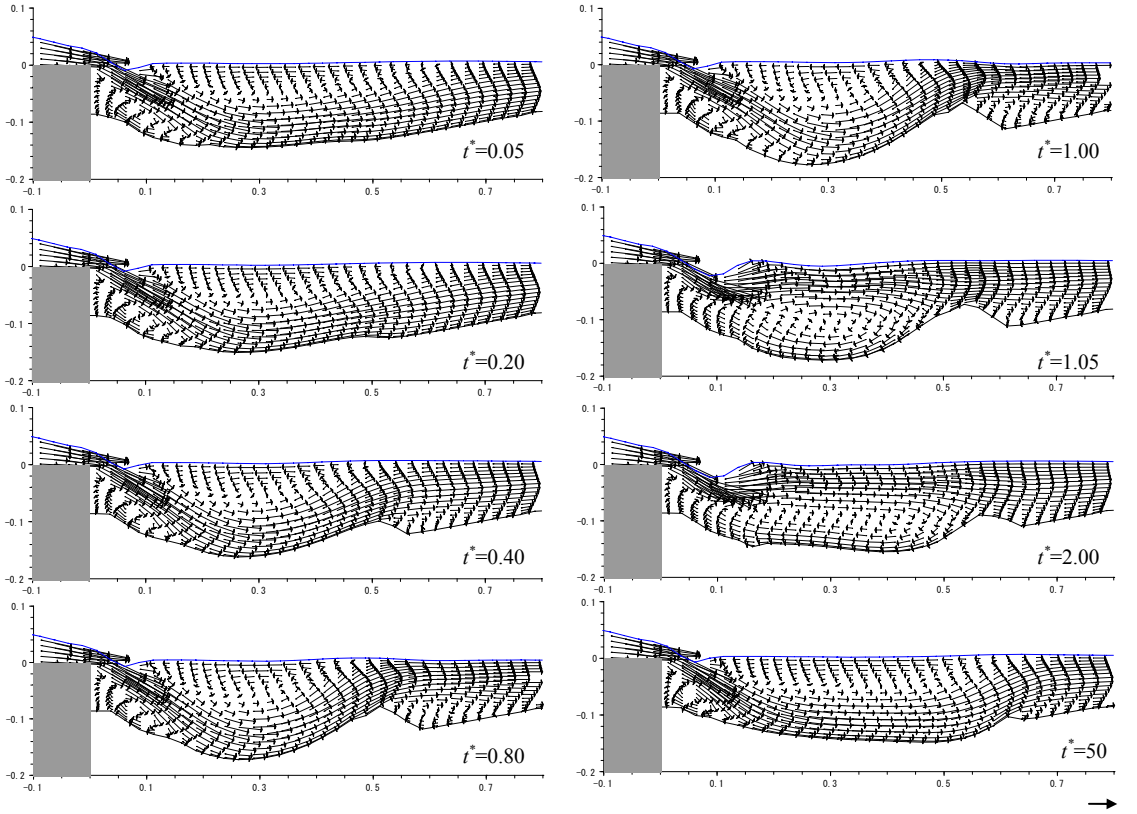

Fig.10 The calculated flow field in the local scour and the transition process of the local scour

angle is made to have the repose angle in the calculation. The initial condition (t=0.0s) for the computation of the local scour is given as the calculated flow field for a submerged jet flow over the measured bed shape (see Fig.6). The relative time t^* is defined as the non-dimensionalized duration time by the submerged jet t_m ($t^*=t/t_m$). The deformation of scour shape is limited to as shown in Fig.9.

Fig.10 shows a series of the calculated flow field in the transition process of the local scour. The sand just downstream of the groundsill is transported towards upstream and downstream soon after the flow has changed into a submersed jet (t^*=0.05). Since the pressure at downstream of a groundsill is decreased by bed scouring, the reattachment point moves in the upstream direction (t^*=0.20). Then a dune is produced in the downstream part of the local scour with the flow separation on the top of the dune (t^*=0.40). After that, the maximum scour depth becomes deeper with time, moving the top of the dune towards downstream (t^*=0.80, 1.00). The reattachment point of flow, after the flow has changed into a wave-jump, moves to

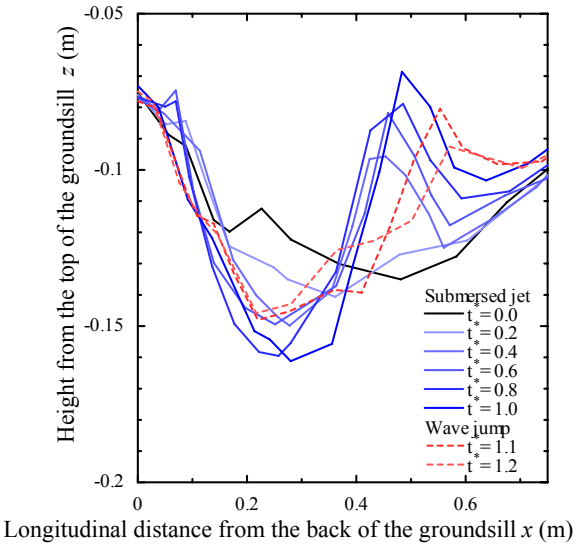

(a) Measured

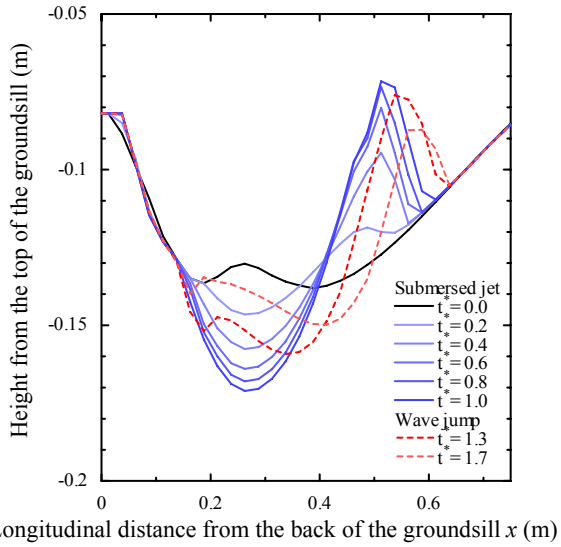

(b) Computed

Fig.11 The transition process of the local scour in just downstream of the groundsill

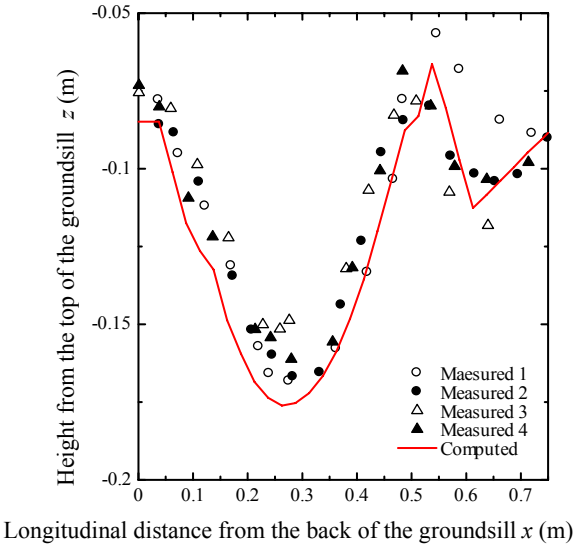

Fig.12 The comparison of maximum depth of the local scour

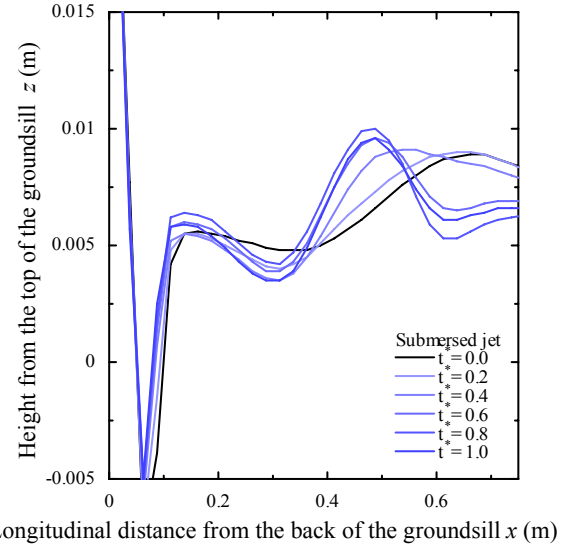

Fig.13 The transition process of the water surface in just downstream of the groundsill by computation

the top of the dune, and then the local scour decays due to reverse flow (t^*=2. 00). The present numerical model can explain both processes. It is also made clear in the computation that after the long duration of the decaying process under wave jump flow, the bed shape enter the developing process with a submerged jet, which is similar to the experiment (t^*=50).

Fig.11 shows the transition processes of the local scour in (a) the measurement and (b) computation. Fig.12 shows the shapes of the local scour at the time when the flow change from a submersed jet to a wave jump. Various shapes of the local scour are measured in the similar flow condition. This results from the instability of the flow transition phenomenon, which involves the transition to a wave jump from a submersed jet and to a submersed-jet from wave jump. However, the scour shape past the groundsill upto the top of the dune is similar. Therefore, the phenomenon that the flow changes from a submerged jet to a wave jump is subject to the effects of shape in this region. Since the shape of the back side of the dune is decided by the repose angle of the sand, the calculated dune is a little smaller than that

of the measurement, and no sand is transported toward the downstream of the local scour. It is safe to say that the present model reproduces the scour shape from the groundsill to the top of the dune, which is subject to the developing process of the local scour as indicated above. And the maximum bed scour depth for the experiment is reproduced by this computation.

Fig.13 shows the calculated transition process of water surface just downstream of the groundsill. The water surface just downstream of the groundsill goes down due to bed scour at that cross-section soon after that the flow has become a submersed jet. Then the profile of the water surface is produced at the backward of the bed wave profile (compare Fig.11 (b)). The water surface at downstream part of the local scour goes down due to the dune formation with the flow separation. Then, the reverse flow area under the water surface is decreased with time, because fluid momentum is transported toward water surface with the developing of the dune. Therefore, the wave profile of the water surface goes upstream, although the wave profile of the bed goes downstream. Then the phase difference of wave profiles between the water surface and the bed shape is reduced. The transition from a submersed-jet to a wave jump occurs when the wave profile of the water surface is laid a little forward of the bed wave profile.

As mentioned above, sediment transportation process on the local scour bed under plunging jet shows large difference from that calculated by equilibrium sediment transport models because of the existence of the pressure fluctuations and suspended sediment. The present model assuming equilibrium sediment transport is, however, successful in predicting scour process and the maximum scour depth. The reason is that the scour process in the present condition is produced directly by the longitudinal distribution of bed shear stress. In other words, it is important to predict local scour process with a submerged jet that the bed shear distribution is computed by a reliable model for the flow, which can represent the vertical velocity distribution in the local scour.

6 CONCLUSION

1. A vertical two-dimensional model, which employs the sigma coordinate system to take into account of the variation of water surface and bed height, is developed. The calculation near the boundary is designed to evaluate abrupt change of the boundary shape.
2. The transition to wave jump and submersed jet flow can be computed by the present model. And it can explain the two different characteristics of the velocity distribution near the bed.
3. The developing process of the local scour under the submerged jet flow and the decaying process with the formation of wave jump flow are reproduced in the computation. The maximum depth of local scour that occurs at the time when the flow pattern changes from submersed jet to wave jump is reproduced by the model. And it is clarified that to predict local scour process with a submerged jet it is quite important to evaluate the bed shear distribution and the vertical velocity distribution in the local scour.

REFERENCES

Ashida, K. and Michiue, M. (1972) Study on hydraulic resistance and bed-load transport rate in alluvial streams, *Proceedings of the Japan Society of Civil Engineers*, No. 206, pp.59-69, in Japanese.

Bormann, N.E. and Julien, P.Y. (1991) Scour downstream of grade-control structure, *Journal of Hydraulic Engineering*, *ASCE,* Vol.117, No.5, pp.579-594.

Kanda, K., Muramoto, Y. and Fujita, Y., (1996) Local scour and its reduction method in downstream of bed protection work, *Journal of hydraulic, coastal and environmental engineering, JSCE*, No.551/II-37, pp.21-36, in Japanese.

Farhoudi, J. and Smith, K. V. H. (1985) Local scour profiles downstream of hydraulic jump, Journal of Hydraulic Research, IAHR, Vol.23, No.4, pp.343-358.

Fukuoka, S. and Yamasaka, M. (1983) Alternating bars in a straight channel, *Proceedings of the Japanese conference on hydraulics*, *JSCE*, pp.823-828, in Japanese.

Hirt, C. W. and Cook, J.L.(1972) Calculating three-dimensional flows around structures and over rough terrain, *Journal of computational physics*, Vol.10, pp.324-340.

Hirt, C. W., (1992) Volume-fraction techniques: powerful tools for wind engineering, *Journal of Wind engineering*, No.52, pp.333-344.

Hoffmans, G. J. C. M. and Booij, R.(1993) Two-Dimensional Mathematical modelling of Local-Scour Holes, *Journal of Hydraulic Research, IAHR*, Vol.31, No.5, pp.615-634.

Hoffmans, G.J.C.M. (1998) Jet scour in equilibrium phase, *Journal of Hydraulic Engineering, ASCE*, Vol.124, No.4, pp.430-438.

Jia, B., Kitamura, T., and Wang, S.S.Y. (2001) Simulation of scour process in plunging pool of loose bed-material, *Journal of Hydraulic Engineering, ASCE*, Vol.127, No.3, pp.219-229.

Kawashima, M. and Fukuoka, S. (1995) Numerical simulation of bed variation around a groundsill, *Annual Journal of Hydraulic Engineering*, *JSCE*, vol.39, pp.689-694, in Japanese.

Mazurek, K.A. and Rajaratnam, K. (2005) Erosion of sand beds by obliquely impinging plane turbulent jets, *Journal of Hydraulic Research, IAHR*, Vol.43, No.5, pp.567-573.

Noel E. Bormann and Pierre Y. Julien(1991) Scour downstream of grade-control structures, *Journal of Hydraulic Engineering, ASCE*, Vol.117, No.5, pp.579-594.

Smagorinsky, J. (1963) General circulation experiments with the primitive equations, *Monthly weather review*, Vol.91, No.3, pp.99-164.

Suzuki, K., Michiue, M. and Kawatsu K. (1982) Study on the local scour and flow downstream of a consolidation work, *Annual Journal of Hydraulic Engineering*, *JSCE*, vol.26, pp.75-80, in Japanese.